Teilprojekt B1.8 (originally B2.14)

Electronic Properties of Graphene Nanostructures

Principal Investigators: Alexander Mirlin and Igor Gornyi

CFN financed scientists: Ivan Dmitriev, Dmitry Gutman, Mikhail Titov

Further contributing scientists: Soumya Bera, Roman Gellmann, Pavel Ostrovsky, Dmitry Polyakov, Alexander Schuessler

Institut für Theorie der Kondensierten Materie
Karlsruher Institut für Technologie, Campus Süd

Institut für Nanotechnologie
Karlsruher Institut für Technologie, Campus Nord

Introduction

Graphene [1] is a particularly intriguing two-dimensional structure with the quasi-relativistic dispersion law that has recently burst into the solid state physics. In 2004, researchers of Manchester University (UK) have succeeded to manufacture a monoatomic graphite layer --- graphene --- on an insulating substrate [2,3,4,5]. This technological breakthrough has attracted a great deal of attention of leading experimental and theoretical groups over the world. In a very short time, a new area of research --- the study of graphene-based structures --- has emerged and become one of key research directions in the material science and condensed matter physics, see Ref.7 for a review. The reason for this is exceptional properties of graphene that make this material highly interesting from the point of view of both fundamental physics and potential applications [1], most prominently, the carbon-based nanoelectronics. A.Geim and K. Novoselov were awarded the Nobel Prize 2010 for the discovery of graphene.

The project is intended to develop a comprehensive theoretical picture of electronic transport in graphene structures, involving all the key ingredients of modern nanoscience: namely, quantum interference, quantum criticality, disorder-induced mesoscopic fluctuations, and Coulomb correlations. The emphasis is put on transport properties of disordered two-dimensional graphene-based systems; the localization and strong correlations in quasi-2D (multi-layers) and quasi-1D systems such as graphene nanoribbons and carbon nanotubes are also studied within the project. The objectives of the project are expected to be particularly relevant to the rapidly growing field of nanotechnology, especially in the emergent carbon-based nanoelectronics.
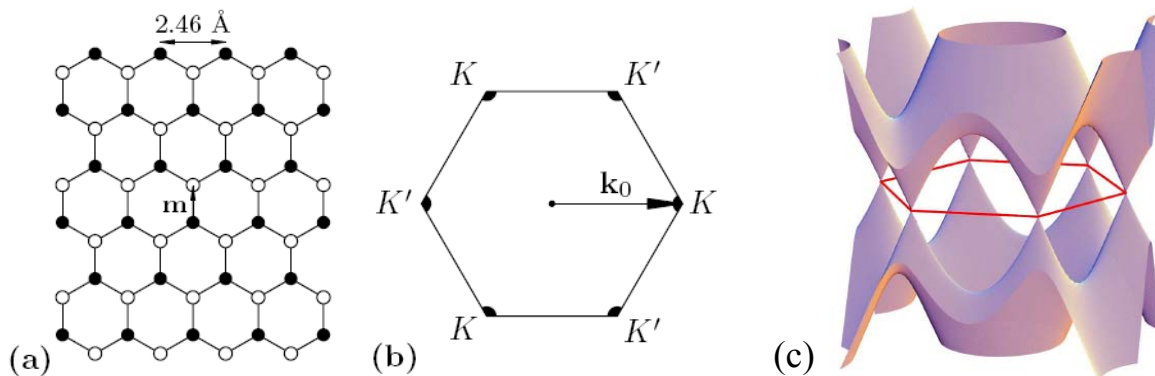
Fig. 1. (a) Honeycomb graphene lattice consists of two sublattices A and B (open circles and dots); (b) Brillouin zone (two valleys are denoted as K and K'); (c) graphene bandstructure.

A hallmark of graphene is its unconventional electronic spectrum (Fig. 1). Specifically, low-energy excitations in graphene are "relativistic" Dirac fermions, with an effective "light velocity" 10^6 cm/s. This leads to remarkable electronic properties of this material that have been revealed by transport measurements [1,4,5]. In particular, graphene shows anomalous, half-integer quantum Hall effect, which is observed up to room temperature, whereas it disappears at 30 K in the best semiconductor structures. Another remarkable discovery is that the conductivity of the undoped (zero gate voltage) graphene in a broad temperature range (from 300 K down to 30 mK) is essentially independent of temperature and has a value close to the quantum e^2/h (times four, which is the total spin and valley degeneracy).

From the point of view of application, it is important that the electron concentration can be varied by a gate, so that graphene can be used to realize a field-effect transistor. Further, a gap can be engineered and tuned in graphene-based structures. Moreover, it appears to be possible to realize a room-temperature single-electron transistor on the basis of graphene [1]. These findings open a way for developments of novel graphene-based electronics [1]. In addition to the nanoelectronics, the extraordinary electronic, thermal, and mechanical properties of graphene allow for various further applications [1], such as composite materials and sensors for individual molecules. Study of electronic transport in disordered graphene will lead to the major advancement in understanding of fundamental properties of systems with quasi-relativistic carriers, including localization, quantum criticality, and a novel type of the quantum Hall effect. This is expected to become a new paradigm in the modern condensed-matter physics and promote the development of a new, graphene-based, nanoelectronics.

We have started to work on electronic properties of graphene in the early 2006, within the CFN project B2.11. Our central achievement [6] ([B2.11:6]) was development of the theory of transport in graphene in the presence of different types of disorder. We have shown that the character of randomness (strength of scatterers and valley/sublattice symmetries) is of crucial importance for transport properties of graphene. Specifically, it is important (i) whether the individual scatterers are strong or weak and (ii) what is the symmetry of the disorder in the sublattice and valley space. We have used a combination of theoretical approaches, including self-consistent Born approximation, self-consistent T-matrix approximation, and renormalization group. Within the renormalization group approach, we have determined a complete set of one-loop equations governing the evolution of coupling constatnts for all symmetries of disorder with the length on ballistic scales.

We have shown, that, away from half filling, the concentration dependence of conductivity is linear (with logarithmic corrections) for strong scatterers (unitary limit), $\sigma \sim n_e \ln n_e$, while it is only logarithmic in the case of weak scatterers (Gaussian disorder). We have constructed a "phase diagram", showing which of these types of behavior should be expected for given microscopic parameters of the disorder. For the physically important case of Coulomb impurities and ripples, which are characterized by long-range $1/r$ potentials, the conductivity behavior is linear as for strong imurities (but without logarithmic correction), $\sigma \sim n_e$. The linear behavior of the conductivity obtained for strong and long-rang scatterers agrees with the experimental findings, demonstrating that one of these kinds of disorder is dominant in experimentally studied structures.

Starting from the year 2007, the graphene-related activity was split into a separate CFN project --- the present one (originally B2.14, since 2009 B1.8).

1. Conductivity of disordered graphene at half filling

In Refs. [B2.14:1, B2.14:2] we have studied electron transport properties of graphene with different types of disorder at half filling. We have shown that the transport properties of the system depend strongly on the symmetry of disorder. We have demonstrated that the localization properties of graphene are governed by the chiral (C), time-reversal (T), and valley (Λ) symmetries of disordered graphene Hamiltonian, in combination with the nontrivial topology of Dirac fermions.

We have identified two broad classes of randomness in graphene --- chiral disorder (preserving chiral symmetry of clean graphene) and long-range disorder (not mixing the two valleys) --- leading to the lack of localization and emergence of quantum criticality and associated universal minimal conductivity (see Table 1). We have obtained the exact value of minimal conductivity $4e^2/\pi h$ in the case of chiral disorder. For long-range disorder (decoupled valleys), we have derived the effective

field theory --- the nonlinear sigma-model. In the case of smooth random potential, it is a symplectic-class sigma model including a topological term with $\theta = \pi$. As a consequence, the system is "topologically protected" from Anderson localization, in line with the remarkable experimental finding. We have proposed the two scenarios (see Fig. 2, right panel): either the system is at a quantum critical point with a universal value of the conductivity of the order of e^2/h, or the conductivity grows with increasing the system size towards the perfect metal. Recent numerical simulations [8] have supported the second scenario.

When the effective time reversal symmetry is broken, the symmetry class becomes unitary, and the conductivity acquires the value characteristic for the quantum Hall transition. Using the derived field theories, we have proposed the beta-functions governing the scaling of the conductivity in the unitary (charged impurities + ripples) and symplectic (charged impurities) symmetry classes, see Fig. 2.
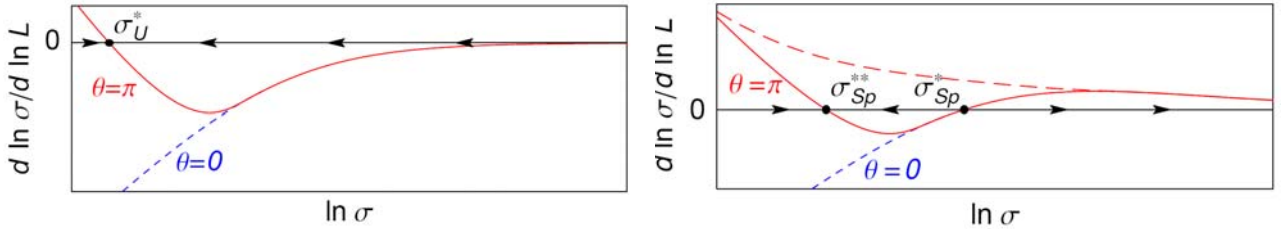
Fig. 2. Renormalization group flows for unitary (left) and symplectic (right) universality classes. Red lines correspond to the sigma models with $\theta = \pi$ topological term; dashed lines correspond to $\theta = 0$. In the symplectic case (charged impurities, right panel), the two scenarios are possible: either with a new critical point σ^{**}_{Sp} (solid line) or with an always positive beta-function (long-dashed line).

Table 1. Possible types of disorder in graphene leading to a finite minimal conductivity. Each row of the table corresponds to a certain universality class of the problem. In the first column we give an example of the disorder that belongs to this class (RMF is an external random magnetic field). The relevant symmetries are placed in the second column. The symmetry class itself is indicated in the third column according to the classification of Altland and Zirnbauer. The fourth column displays the dominant non-trivial term in the corresponding sigma model. This term is responsible for the absence of localization. There are three possibilities: (i) Gade term, (ii) Wess-Zumino-Witten term, or (iii) Pruisken θ-term with $\theta = \pi$. The value of the minimal conductivity is given in the last column. The first five rows contain chiral-symmetric types of disorder [ripples can be added to any of them]. They all yield the minimal conductivity $4e^2/\pi h$ (up to power-law corrections in a weak disorder strength for C_z chirality, hence "$\approx$"). The last four rows correspond to the case of decoupled valleys (long-range disorder); from top to bottom: random Dirac vector potential, scalar potential, mass, and any of their combinations. The value of the minimal conductivity depends on a particular symmetry of the long-range disorder.

| Disorder	Symmetries	Class	Sigma model	Conductivity
Vacancies, strong potential impurities	C_z, T_0	BDI	Gade	$\approx 4e^2/\pi h$
Vacancies + RMF	C_z	AIII	Gade	$\approx 4e^2/\pi h$
$\sigma_3\tau_{1,2}$ disorder	C_z, T_z	CII	Gade	$\approx 4e^2/\pi h$
Dislocations	C_0, T_0	CI	WZW	$4e^2/\pi h$
Dislocations + RMF	C_0	AIII	WZW	$4e^2/\pi h$
Ripples, RMF	Λ_z, C_0	$2\times$AIII	WZW	$4e^2/\pi h$
Charged impurities	$\Lambda_z, T_\perp$	$2\times$AII	$\theta = \pi$	$\sim 4e^2/h$ or ∞
random Dirac mass: $\sigma_3\tau_0, \sigma_3\tau_3$	$\Lambda_z, CT_\perp$	$2\times$D	$\theta = \pi$	$4e^2/\pi h$
Charged impurities + (RMF, ripples)	Λ_z	$2\times$A	$\theta = \pi$	$(0.5 - 0.6) \times 4e^2/h$

.

Remarkably, Dirac fermions in graphene with different types of disorder may give rise to all possible types of criticality emerging in the context of Anderson localization in 2D systems, see our recent review Ref. [9].

2. Theory of Anomalous Quantum Hall Effects in Graphene

The key feature of graphene is the massless Dirac type of low-energy electron excitations (Fig. 1). This gives rise to a number of unusual physical properties of this system distinguishing it from conventional two-dimensional metals. One of the most remarkable properties of graphene is the anomalous quantum Hall effect. It is extremely sensitive to the structure of the system; in particular, it clearly distinguishes single- and double-layer samples.

In Ref. [B2.14:7] we have developed the theory of disordered graphene in strong magnetic fields (quantum Hall regime). We have demonstrated that the Landau level structure by itself is not sufficient to determine the form of the quantum Hall effect (QHE). The Hall quantization is due to Anderson localization which, in graphene, is very peculiar and depends strongly on the character of disorder. It is only a special symmetry of disorder that may give rise to anomalous quantum Hall effects in graphene.

We have concentrated on the experimentally relevant case when the randomness preserves one of the chiral symmetries of the clean Hamiltonian and/or does not mix valleys. In particular, a disorder model dominated by ripples (random distortions in a honeycomb lattice) has been analyzed. Another disorder model which we have investigated is that of Coulomb impurities, with dominant intravalley scattering. According to our recently developed classification [6, B2.14:2], ripples represent the chiral type of disorder, whereas the charged impurities in the absence of magnetic field belong to the symplectic symmetry class owing to the pseudospin structure of Dirac Hamiltonian. Further, both models give rise to non-trivial topological properties of the corresponding low-energy theory. The topology manifests itself in the experimentally observed half-integer quantization of the Hall conductivity. We have also studied how a weak intervalley scattering induces a crossover from the half-integer to the integer QHE with lowering temperature.
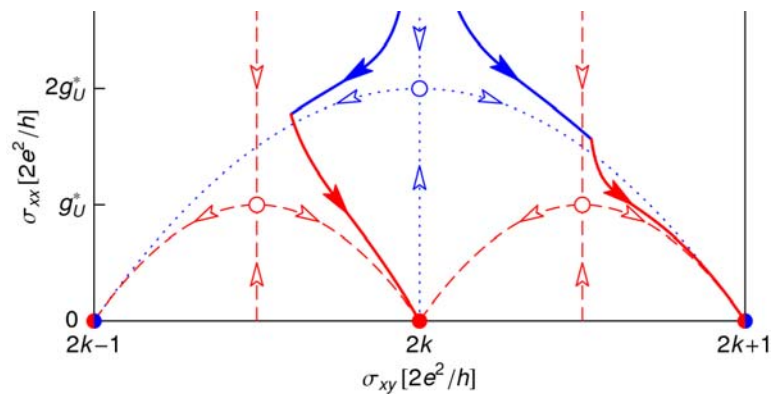
Fig. 3. Renormalization group flow of σ_{xx} and σ_{xy} in graphene with decoupled and mixed valleys. Dotted/dashed lines are separatrices of the flow for graphene with decoupled/mixed valleys. Open circles are unstable fixed points corresponding to quantum Hall transitions. Stable fixed points (plateaus) are shown as disks. Two solid curves demonstrate a possible flow towards even- and odd-plateau fixed point for a model with weakly mixed valleys. Each curve has a cusp when the running scale reaches the intervalley scattering length.

Using the sigma-model formalism and the renormalization group approach (Fig. 3), we have analyzed the symmetries of disordered single- and double-layer graphene in magnetic field and identified the conditions for anomalous Hall quantization. Specifically:
(i) a smooth random (scalar) potential which does not couple the valleys gives rise to the odd QHE, dashed line in Fig. 4 (left);
(ii) the valley mixing splits the odd quantum Hall transitions and restores the ordinary Hall quantization, solid line in Fig. 4 (left). For weakly mixed valleys the crossover from the odd to ordinary QHEs occurs at parametrically low temperatures, Fig. 4 (right). We have estimated the crossover temperature for the realistic model of Coulomb impurities as $T \sim 100$mK, which is still accessible in experiments on graphene;
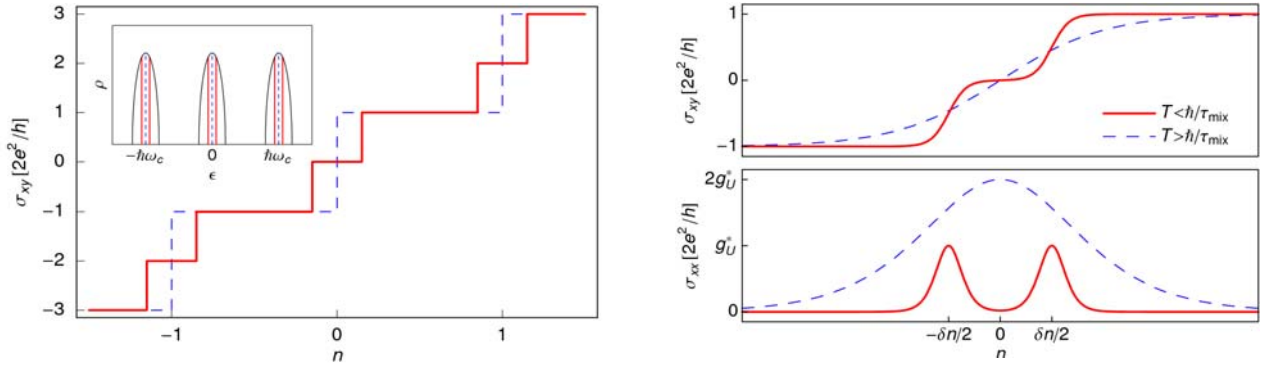
Fig. 4. *Left panel:* Quantum Hall effect in graphene with smooth disorder at zero temperature. Hall conductivity as a function of the filling factor n: odd (decoupled valleys, dashed line) vs normal (weak valley mixing, solid line) quantization. Inset shows the energy dependence of the density of states. The state in the center of Landau level is delocalized (dashed lines) when the valleys are decoupled. The valley mixing splits this delocalized state (solid lines).
Right panel: Quantum Hall transition at finite temperature. A double step in σ_{xy} and a double peak in σ_{xx} (solid lines) require temperature lower than the intervalley scattering (mixing) rate. Otherwise a single broadened quantum Hall transition is seen (dashed lines).

(iii) ripples or dislocations (random vector potential preserving the chiral symmetry) lead to a "classical" QHE with the linear dependence of σ_{xy} on the filling factor, Fig. 5 (left), around the half filling;
(iv) in double-layers, a double-step QHE transition at zero carrier concentration arises for disorder smooth on the scale of magnetic length, Fig. 5 (right).
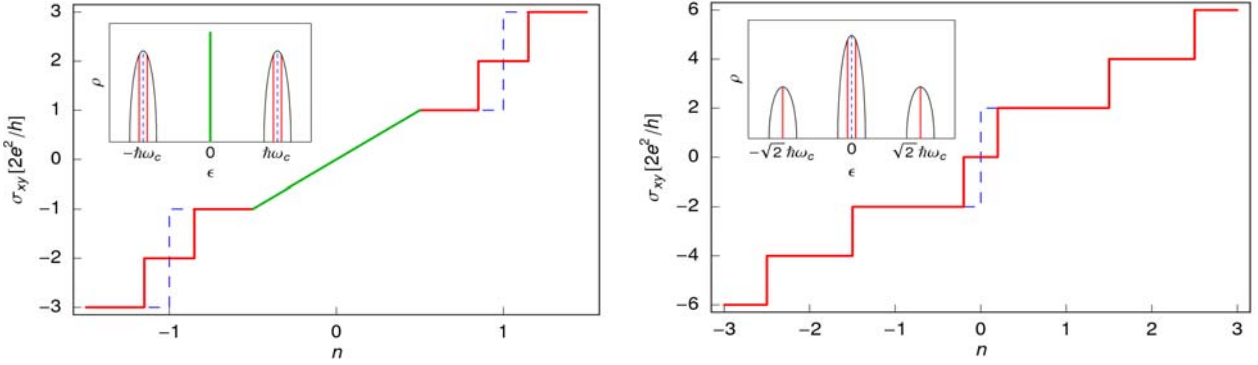
Fig. 5. *Left panel:* "Classical" QHE in graphene with chiral disorder (random vector potential). Chiral symmetry protects degeneracy of the lowest Landau level (Inset: delta-function in the density of states). Hall conductivity is a linear function of carriers concentration while the lowest Landau level is being filled. In Abelian case (ripples) only odd plateaus appear away from zero energy (dashed line). Non-Abelian gauge disorder (dislocations) split quantum Hall transitions as shown by solid line.
Right panel: QHE in a double-layer graphene with smooth disorder (decoupled valleys). Degeneracy of the lowest Landau level is twice larger than for other levels. Double step at zero filling factor (dashed line) is split when the disorder has finite correlation length d. Inset shows the density of states and positions of delocalized states (solid lines). Two such states within the lowest Landau level are degenerate (dashed line) in the limit of infinite d.

Experiments on QHE in graphene thus provide information about the nature of disorder. The observation [4,5] of the odd-integer QHE represents a direct evidence in favor [B2.14:7] of smooth potential disorder which does not mix the valleys (Coulomb impurities). This also explains the absence of localization at zero magnetic field, as shown in Refs. [B2.14:1, B2.14:2].

### 3. Ballistic transport in disordered graphene

In Ref. [B1.8:1, B1.8:2], we have developed the analytic theory of electron transport in disordered graphene in a ballistic geometry. In this paper, we have analyzed transport properties of a graphene sample in the "wide and short" geometry ($W >> L$, Fig. 6), with disorder effects restricted to intra-valley scattering. This setup allows one to define the "conductivity" $\sigma = G L / W$ even for ballistic samples with L much shorter than the mean free path l. Remarkably, in graphene at the Dirac point, such ballistic "conductivity" has a universal value $4e^2/\pi h$ in the clean case [10]. This setup was studied experimentally in Ref. [11] and the ballistic value $4e^2/\pi h$ was indeed observed for large aspect ratios. This geometry of samples is particularly advantageous for the analysis of evolution from the ballistic to diffusive transport.
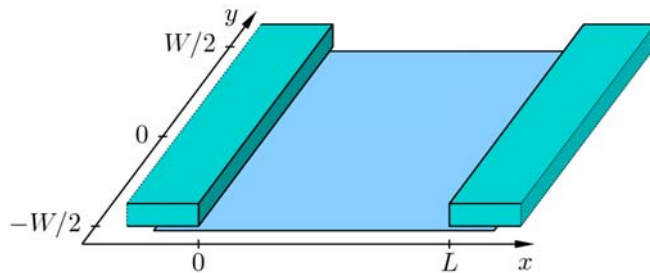
Fig. 6.   Schematic setup for two-terminal transport measurements. Graphene sample of length L and width W is placed between two parallel contacts.

A complete description of the electron transport through a finite system involves not only the conductance but also higher cumulants of the distribution of transferred charge. The second moment is related to the current noise in the system. The intensity of the shot noise is characterized by the Fano factor F. For clean graphene, this quantity was studied in Ref. [10]. Surprisingly, in a short and wide sample ($W >> L$) the Fano factor takes the universal value $F = 1/3$, that coincides with the well-known result for a diffusive metallic wire. The effect of disorder on the shot noise was studied numerically in Ref. [12], where the value of the Fano factor close to 0.3 was found across the whole crossover form ballistics to diffusion. The Fano factor close to 1/3 was also observed at the Dirac point experimentally [11]. When the chemical potential was shifted away from the Dirac point, the Fano factor decreased, then showed an intermediate shoulder around $F = 0.15$, and finally approached zero for largest gate voltages (carrier concentrations).

While both diffusive and clean limits have been addressed analytically, only numerical and experimental results for the intermediate regime of ballistic transport through disordered samples have been available so far. In Ref. [B1.8:2] we have filled this gap. We have calculated the full statistics of the charge transfer for both zero (the Dirac point) and large concentration of carriers. Starting from the clean limit (Fig. 7) and using the transfer-matrix technique, we have analyzed the evolution of the transmission distribution $P(T)$ and, in particular, of the conductance G and the Fano factor F, with increasing system size L.
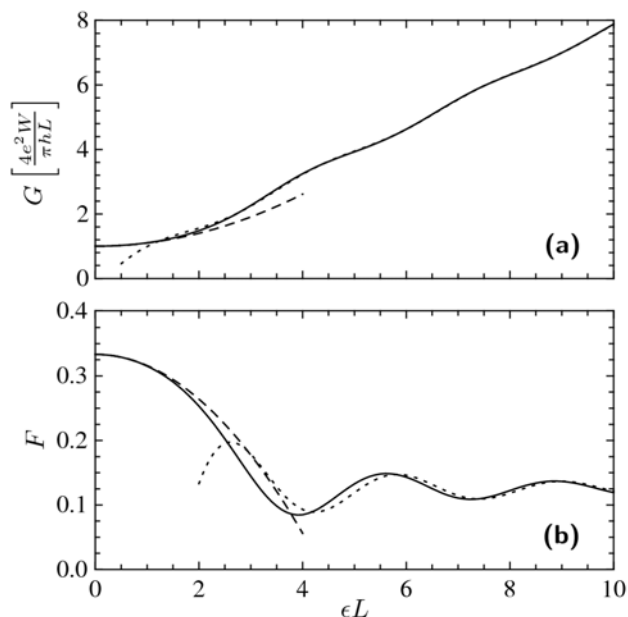
Fig. 7.   Energy dependence of the (a) conductance and the (b) Fano factor of the clean sample with $W >> L$. Solid lines show numerical results. Low energy asymptotics is plotted by dashed lines while dotted lines correspond to high energy limit. Asymptotical curves provide a very good approximation to the exact result in the whole range of energies.
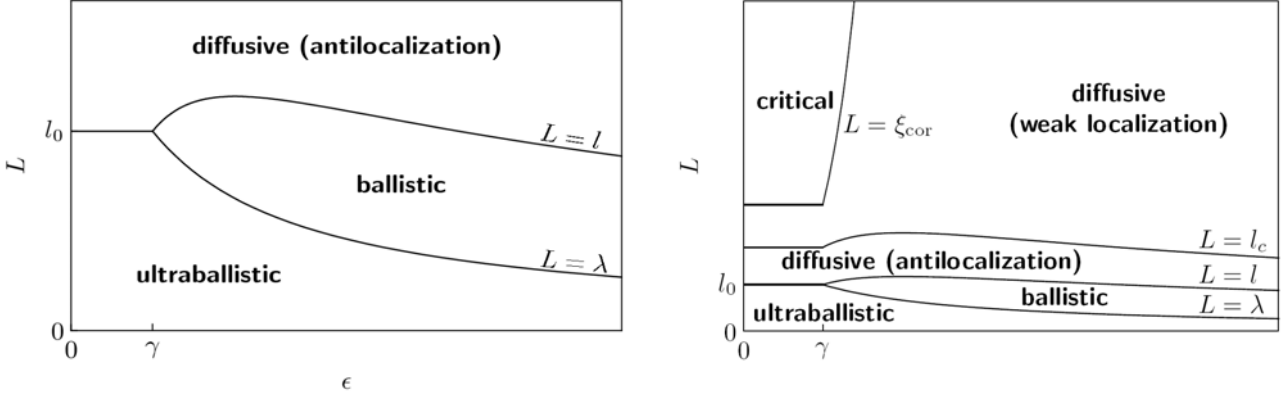
Fig. 8. *Left panel:* Schematic "phase diagram" of various transport regimes in the graphene sample with random scalar potential. The lines indicate crossovers between corresponding regimes. The shortest sample exhibits ultraballistic transport. When the length of the sample exceeds Fermi wave length, ballistic results apply. In a sample longer than the mean free path, diffusive regime establishes with the Drude conductivity and the Dorokhov distribution of transmission eigenvalues. The conductivity experiences antilocalization (symplectic symmetry class) in this case.
Right panel: Schematic "phase diagram" for the case when more than one disorder type is present in the system. The ultraballistic, ballistic, and diffusive (lowest part) regimes are similar to the left panel. Once the diffusion is established, the antilocalization starts but it proceeds only till the length at which the time-reversal symmetry breaks down. At longer scales the system falls into the unitary symmetry class and exhibits weak (second-loop) localization. At exponentially long scale $\xi_{\rm cor}$ the quantum Hall critical state establishes.

To take the randomness into account, we have developed a perturbative treatment of the transfer-matrix equations. This approach has been supplemented by a renormalization-group formalism describing the renormalization of disorder couplings. This has allowed us to get complete analytical description of the transport properties of graphene in the ultraballistic ($L<<\lambda$) and ballistic ($\lambda << L << l$) regimes (here λ is the Fermi wavelength inside the sample and l is the mean free path). We have also constructed "phase diagrams" of different transport regimes (ultraballistic, ballistic, diffusive, and critical) for graphene with various types (symmetries) of intra-valley disorder. In the left panel of Fig. 8 we show the result for potential disorder (e.g., Coulomb impurities); the right panel of Fig. 8 illustrates the transport regimes in the case of generic disorder (e.g., Coulomb impurities plus ripples).

Remarkably, for random scalar potential the transmission distribution function *P(T)* at zero energy appears to be the same in ultraballistic and diffusive limits ("Dorokhov distribution"):

$$P(T) = \frac{W}{2\pi L}\frac{g}{T\sqrt{1-T}},$$

with the dimensionless conductivity $g = (\pi h/4e^2)\sigma$. Taking into account interference effects leads to the L dependence of g in this formula:

$$g = \begin{cases} 1 + 2\alpha_0(L), & \text{ultraballistic,} \\ \dfrac{\pi h}{4e^2}\,\sigma(L), & \text{diffusive,} \end{cases}$$

where $\alpha_0(L)$ characterizes the renormalized strength of disorder.

Most of the available experimental observations [11] reasonably agree with our results. In particular, the Fano factor has a value close to 1/3 at the Dirac point even in the presence of disorder and decreases when one moves away from the Dirac point, showing a tendency to saturate around $F=0.15$, which is not far from the value 1/8 we have obtained in the high-energy regime.

In Ref. [B1.8:10] we have explored the full counting statistics of the charge transport through an undoped graphene sheet in the presence of smooth disorder. At the Dirac point both in clean and diffusive limits, transport properties of a graphene sample are described by the universal Dorokhov distribution of transmission probabilities, see above. In the crossover regime, deviations from universality occur which can be studied analytically both on ballistic and diffusive sides. In the ballistic regime, we used a diagrammatic technique with matrix Green functions and showed that to second order in the disorder strength a correction to the universal counting statistics of the ballistic graphene does arise. We calculated this correction and demonstrated that it suppresses the Fano factor below the value 1/3. Further, we have analyzed the opposite limit of large system size, when the system is in the diffusive regime. Using the sigma model approach, we have identified deviations from the universal distribution in this regime as well. In particular, we have found that that the Fano factor returns to the value of 1/3 from below with increasing L (Fig. 9). The approach to 1/3 is however logarithmically slow. Our results compare well with recent numerical works [12,13].
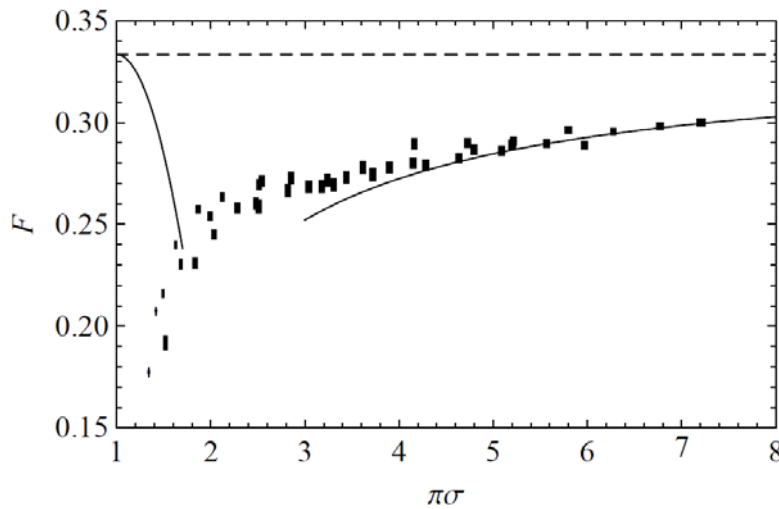
Fig. 9. Fano factor as a function of conductivity. Solid lines show ballistic and diffusive results. Dashed line corresponds to the asymptotic value F = 1/3. Solid symbols are numerical results from Ref. 13, the size of rectangles corresponds to the error estimate.

4. Transport in graphene with resonant scatterers.

Strong scatterers (Fig. 10) produce a dramatic effect on the electron transport. In Refs. [B1.8:8, B1.8;9, B1.8:14], and [14] we have developed a novel general approach to the calculation of various transport properties of the graphene sample with strong impurities. This approach is based on the specifically designed unfolded representation of the scattering matrix of the system. It allows extremely efficient numerical simulations of the electron transport far overperforming the standard method of recursive Green's functions. While complexity of the conductance calculation within the latter approach is polynomial in the system size (e.g., in the number of atoms), the algorithm based on the unfolded scattering matrix representation is polynomial in just the number of impurities.
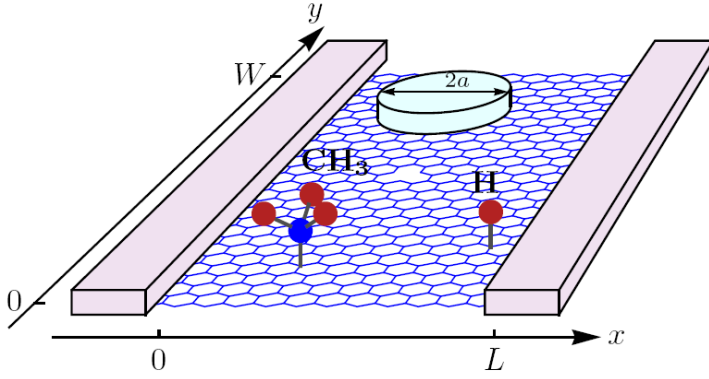
Fig. 10. Ballistic graphene setup with various strong scatterers. Vacancies as well as atomic or molecular impurities can create midgap states. Metallic islands support quasi-bound states that can be tuned to the resonance.

In Ref. [B1.8:8] we have computed the full counting statistics for the charge transport through an undoped graphene sheet in the presence of a small number of strong potential (scalar) impurities. We have considered the ballistic transport regime in which the sample size is smaller than the electron mean free path (low impurity concentration). This model was experimentally implemented in the samples on the SiO_2 substrate. The ballistic transport is particularly relevant for suspended samples where much higher mobilities have been achieved. We have employed the phenomenological scattering approach and complemented it with the microscopic analysis based on the Green functions formalism. Treating the scattering off the impurity in the s-wave approximation, we have calculated the impurity correction to the cumulant generating function. This correction to the full counting statistics is determined by the position of impurity and the low-energy scattering length. The latter diverges when the impurity potential contains a quasi-bound state at zero energy. At such resonant conditions the impurity correction becomes universal. In particular, the conductance of the sample acquires a correction of $16e^2/\pi^2 h$ per resonant impurity, see Fig. 11 (left). Our results are fully supported by numerical simulations with no adjustable parameters, see Fig. 11 (right).
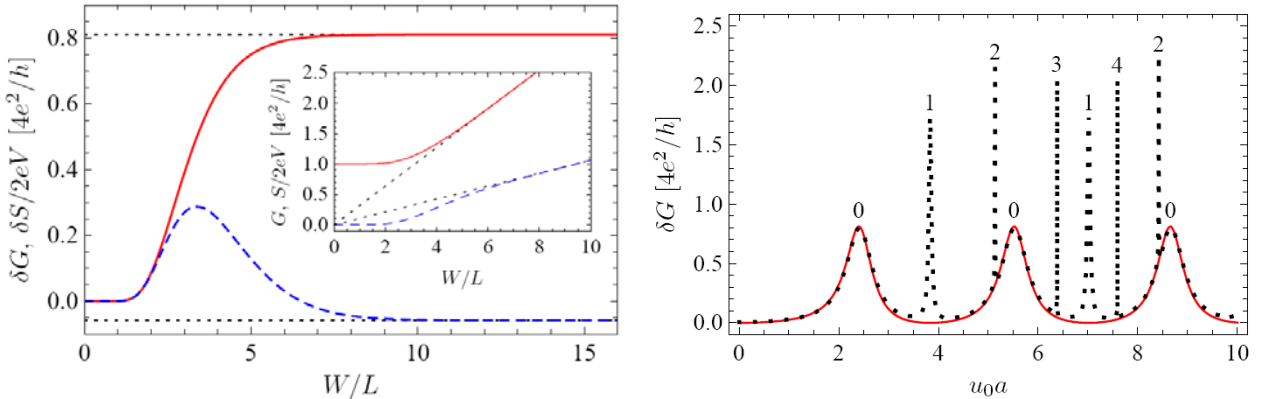

Fig. 11. *Left panel:* Contribution to the conductance G and to the shot noise S from a resonant impurity placed at the center of a rectangular sample (at $x_0=L/2$), as a function of the aspect ratio W/L. Inset: conductance and noise of a clean sample.
Right panel: Correction to the conductance from a circular impurity at $x_0=L/2$ as a function of $u_0 a$ (where u_0 is the height of the impurity potential and a is the radius of impurity). Solid line: numerical simulations [15] with the parameters $a/L = 0.2$, $W/L = 6$; dashed line: analytic result of Ref. [B1.8:8].

In Ref. [B1.8:8] we have studied the effect of resonant scatterers on the local density of states in a rectangular graphene setup with metallic leads. We have found that the density of states in a vicinity of the Dirac point acquires a strong position dependence due to both metallic proximity effect (Fig.

12, left panel) and impurity scattering (Fig. 12, right panel). This effect may prevent uniform gating of weakly-doped samples. We have also demonstrated that even a single-atom impurity may essentially alter electronic states (see Fig. 12, right panel) at low doping on distances of the order of the sample size from the impurity.
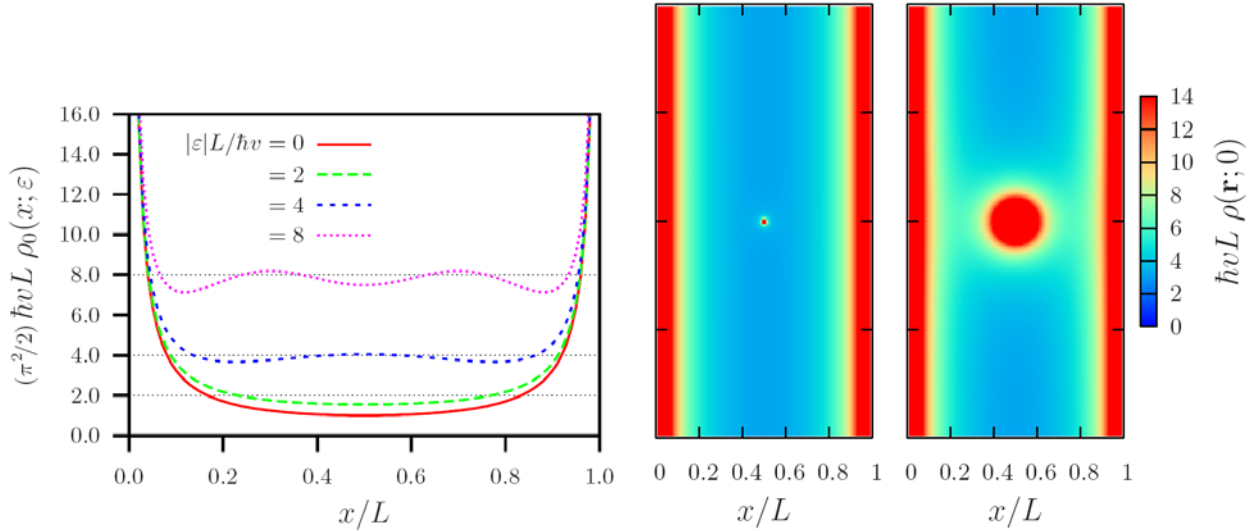
Fig. 12. *Left panel:* The local density of states (LDOS) of Dirac quasiparticles in ballistic graphene sample with metal boundaries and *W/L = 10*. The increase of the LDOS near the boundaries is due to the metallic proximity effect. Different curves correspond to different energy values $\varepsilon L/v$ = 0,2,4,8. *Right panel:* The density plot for the LDOS at ε = 0 for out-of-resonance (left) and resonance (right) conditions. The physical size of impurity is chosen as a = 0.05L, while the effect on the LDOS is determined by the effective scattering length l_s. At resonance conditions, $l_s \gg L$, the LDOS is strongly enhanced in the large area, which is of the order of the system size L.

Using the "unfolded scattering theory", in Refs. [B1.8:14] and [14] we have studied electron transport of graphene with vacancies and revealed a rich phase diagram of various critical transport regimes. One example of critical scaling of conductance in graphene with vacancies is shown in Fig. 13. These results are not attainable with any other known computational tool. Potential further applications of the developed technique are not limited to graphene and include transport characteristic of any disordered systems. This new approach is particularly beneficial for studying systems with strong impurities and, in particular, close to metal-insulator transition, where all other known methods become inefficient.

More specifically, in Ref. [B1.8:14] we have developed a theoretical approach to transport in *disordered* systems which describes an entire crossover from ballistic to diffusive or critical regime. The theory can be applied to study localization physics and criticality in a variety of different systems. We have used the theory to calculate the conductivity (and, more generally, the full counting statistics) in undoped graphene with resonant impurities. The conductivity increases logarithmically in the case of smooth resonant potential scatterers (symmetry class DIII) and saturates at a constant value for vacancies (class BDI), see Fig. 13. In the latter case, the behavior of conductivity depends on the vacancy distribution among the two sublattices (A and B) of the honeycomb lattice with concentrations n_A and n_B. Our results show highly non-trivial scaling flow and phase diagrams of random Dirac fermions in these classes.
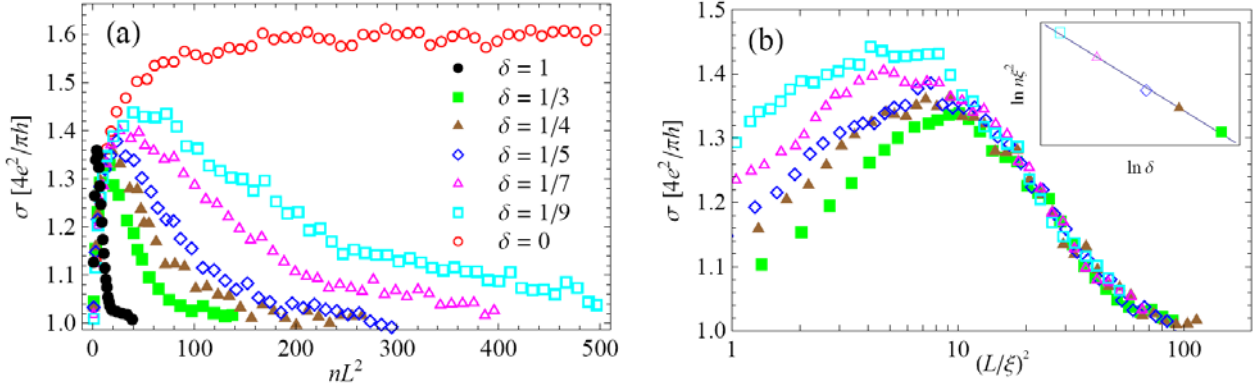
Fig. 13. *Left panel:* Conductivity of graphene as a function of the concentration of vacabcies $n = n_A + n_B$ for various values of $\delta = (n_A - n_B)/n$. *Right panel:* Universal crossover between $n_A = n_B$ and $n_A \neq n_B$ fixed points.

In Ref. [14] we have theoretically proposed and numerically confirmed an extended classification of impurity sites in the graphene honeycomb lattice for the case of strongly-bound adatoms or vacancies. The classification is illustrated in Fig. 14 (left panel) by assigning colors to the lattice sites. The general analytical expression for the Dirac-point conductance of a graphene sample with two resonant on-site impurities is given as a function of impurity coordinates. The Dirac-point conductivity of graphene with a small number of randomly distributed adatoms is shown to be sensitive to the relative concentration of impurities at the sites belonging to different sublattices and having different colors (see Fig. 14, right panel).
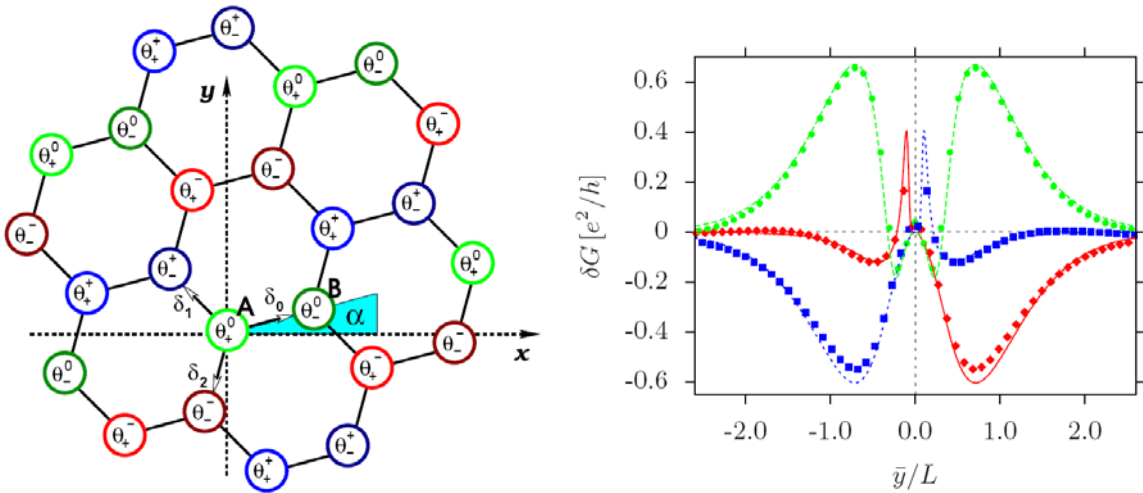

Fig. 14. *Left panel:* Color scheme for vacancies or resonant adatoms. The impurity site is characterized by the phase $\theta_\pm^c = \pm\alpha + 2\pi c/3$ where $\pm$ refers to the sublattice (A or B) and $c = -1, 0, 1$ denotes the colors (red, green, blue). The color scheme depends on the transport direction x. *Right panel:* Conductance variation for an "armchair" sample with two vacancies (A and B). Changing the distance y between vacancies, the conductance jumps on the atomic scale between three different smooth curves corresponding to $\theta = 0$ (green disks), $\theta = 2\pi/3$ (blue

squares), and $\theta = -2\pi/3$ (red diamonds). The numerical data agrees well with the analytical result, as shown by the corresponding solid curves.

5. Graphene-based nanostructures.

In Ref. [B1.8:7] we developed a transfer matrix approach to study ballistic charge transport in few-layer graphene (Fig.15, left) with chiral-symmetric stacking configurations. We demonstrated that the chiral symmetry justifies a non-Abelian gauge transformation at the spectral degeneracy point (zero energy). This transformation proves the equivalence of zero-energy transport properties of the multilayer to those of the system of uncoupled monolayers. Similar transformation can be applied in order to gauge away a spatially dependent magnetic field and/or strain as well as hopping disorder in the bulk of the sample. Further, we calculated, using the scattering approach, the full-counting statistics at arbitrary energy for different stacking configurations (Fig.15, right). The predicted gate-voltage dependence of conductance and noise can be measured in clean multilayer samples with generic metallic leads.
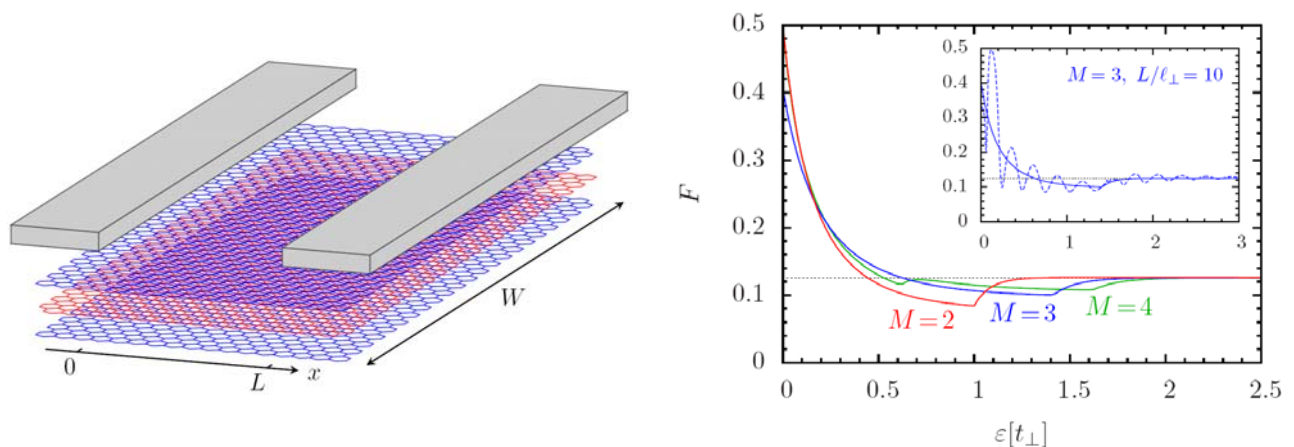

Fig. 15. *Left:* Schematic view of a rectangular trilayer graphene sample contacted by metallic leads. *Right:* Averaged Fano factor (with smeared Fabry-Perot oscillations) vs. chemical potential in transport through AB-stacked few-layer graphene. The horizontal line corresponds to F =1/8. The inset shows a comparison with the exact result (dashed curve) that shows Fabry-Perot oscillations.

In Ref. [B1.8:3] the in-plane resistivity of highly oriented pyrolytic graphite (HOPG) was studied, both experimentally and theoretically. The main focus was on the intermediate temperature range where next-to-nearest plane couplings are irrelevant and graphite can be thought of as a stack of graphene bilayers. We have found that the temperature dependence of the in-plane resistivity is determined by a competition between those of the carrier number density, $n(T)$, and of the scattering rate $1/\tau$. At temperatures below 50 K, the number density is practically independent of the temperature, while the scattering rate increases with the temperature; as a result, the resistivity increases with T. At temperatures comparable to the Fermi energy, the increase in $n(T)$ almost compensates for that in $1/\tau$, leading to a quasisaturation of ρ_{ab} at $T\sim300\ K$. However, full saturation never occurs because, as the temperature increases further, scattering off hard optical phonons, characterized by an exponential increase in $1/\tau$ with T, becomes important. We provide a theory of this effect based on intervalley scattering of charge carriers by high-frequency, graphene-like optical phonons. This results in a further increase in ρ_{ab} with T (Fig.16).
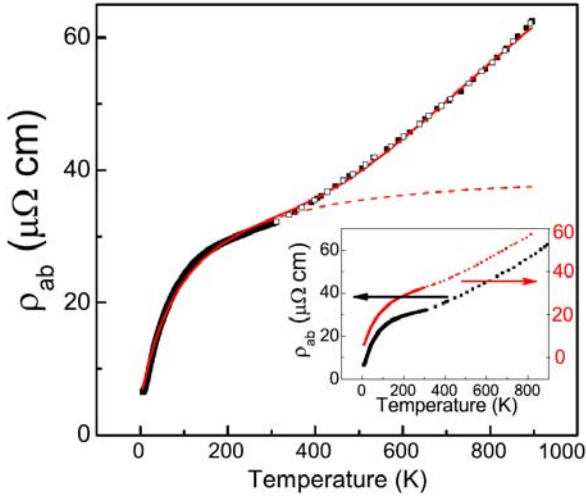
Fig.16. Measured temperature dependence of the in-plane resistivity of HOPG for warming (filled squares) and cooling (blank squares) temperature sweeps. Dashed: theoretical prediction for $\rho_{ab}(T)$ in the model containing scattering at impurities and soft phonons. Solid: fit using the model containing scattering at impurities, soft phonons, and intervalley scattering at hard in-plane optical phonons. Inset: overlap of the data for two different samples. The vertical scales were shifted for clarity.

Motivated by recent proposals on strain engineering of graphene electronic circuits, we studied in Ref. [B1.8:11] conductivity, shot noise and the density of states in periodically deformed graphene (Fig.17). We also proposed a way to characterize the quality of graphene superstructures on the basis of their transport properties. More specifically, we used the Dirac-Kronig-Penney model, which describes the phase-coherent transport in clean monolayer samples with an one-dimensional modulation of the strain and the electrostatic potentials. The exact results were compared to a qualitative band-structure analysis. We found that periodic strains induce large pseudogaps and suppress charge transport in the direction of strain modulation. The strain-induced minima in the gate-voltage dependence of the conductivity characterize the quality of graphene superstructures. The effect is especially strong if the variation in interatomic distance exceeds the value a^2/l, where a is the lattice spacing of free graphene and l is the period of the superlattice. A similar effect induced by a periodic electrostatic potential is weakened due to Klein tunnelling.
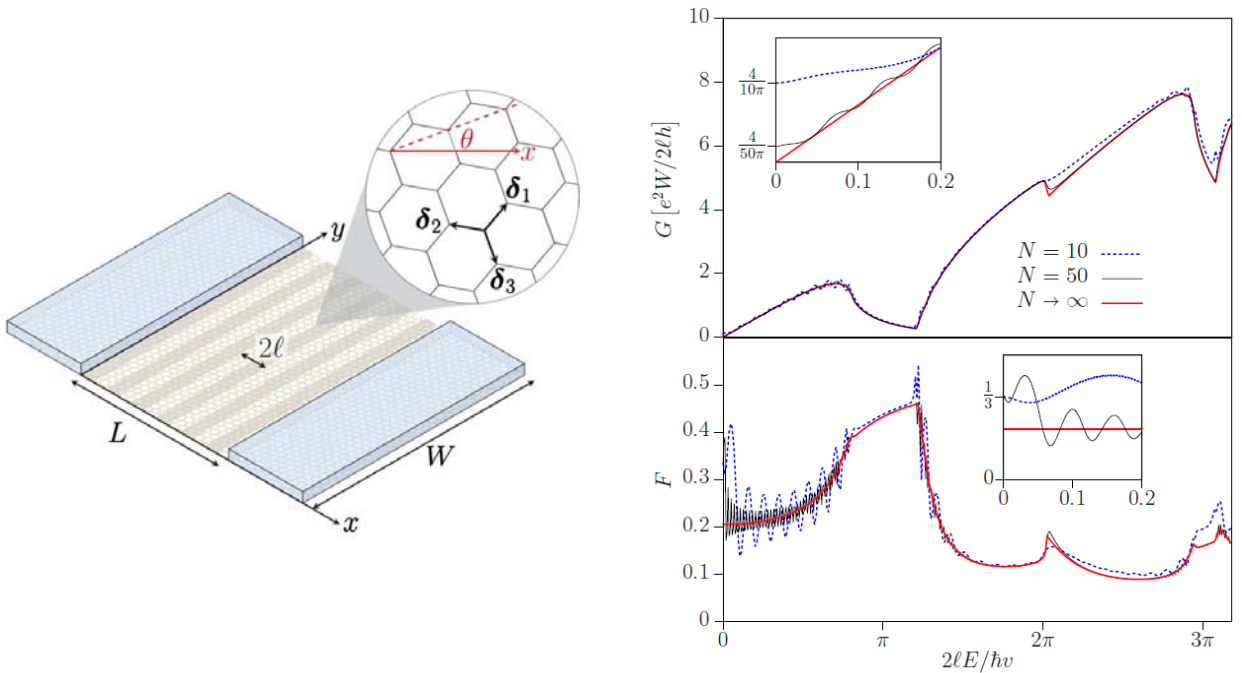

Fig.17. *Left:* Schematic illustration of the strain-modulated graphene setup with metal leads for $x < 0$ and $x > L$. The angle θ specifies the orientation of the honeycomb lattice with respect

to the transport direction x. *Right:* Conductance and Fano factor for finite samples of strain-modulated graphene comprising $N=10$ and $N=50$ supercells. Also shown are averaged expressions which correspond to the limit $N\rightarrow\infty$ and ignore contributions from evanescent modes. In a small vicinity of the Dirac point (shown at the insets) the transport is insensitive to strain due to the extended gauge invariance and is dominated by the evanescent modes.

6. Coulomb interaction in graphene: Relaxation rates and transport

In Ref. [16], we have analyzed the inelastic electron-electron scattering in graphene using the Keldysh diagrammatic approach. We have demonstrated that finite temperature T strongly affects the screening properties of graphene. This, in turn, dramatically influences the inelastic scattering rates as compared to the zero temperature case. We have calculated the finite-T quantum scattering rate, Fig. 18 (left panel), which is relevant for dephasing of interference processes. We have identified an hierarchy of regimes, arising due to the interplay of a plasmon enhancement of the scattering and finite-temperature screening of the interaction. The lifetime of quasiparticles with energies close to the Dirac point has been found to be independent of the coupling constant. We have further calculated the energy relaxation rate and transport scattering rate, Fig. 18 (right panel). For all the three rates, we have found a non-monotonic energy dependence which has been attributed to the resonant excitation of plasmons. Finally, we have discussed the collision-limited conductivity of clean graphene as well as the expected behaviour of the high-temperature conductivity in the presence of disorder,. Our results complement the kinetic-equation and hydrodynamic approaches for the collision-limited conductivity. Our approach that employs the Keldysh formalism can be generalized for the treatment of physics of inelastic processes in strongly non-equilibrium setups. In particular, this framework is expected to allow us to investigate interaction effects on full counting statistics of the electron transport in graphene and to develop the theory of tunneling spectroscopy in strongly biased graphene setup.
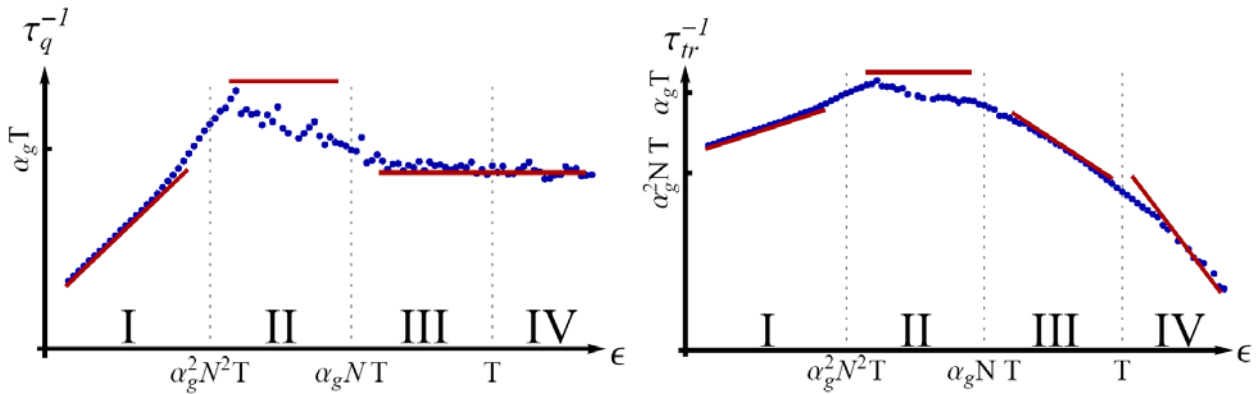

Fig. 18. Quantum scattering rate (left panel) and transport scattering rate (right panel) due to the Coulomb repulsion in clean graphene for $= 4 \times 10^{-3}$ (double logarithmic scale), where $\alpha_g = e^2/v_F$ and N is the number of independent flavours (valleys, spin). Dots: exact values obtained by numerical evaluation; solid lines: analytical asymptotics.

7. Optoelectronic and nonequilibrium properties of 2D electronic gases

One of directions of our current and planned graphene research are optoelectronic and nonequilibrium properties of graphehe-based nanostructures. This will open a number of fascinating possibilities, including controlled modfication of the Dirac spectrum by external fields

(optical driving or/and gate modulations), such as opening of spectral gaps, confinement of carriers, instabilities and quantum generation. It is very important to understand similarity and differences between graphene and more conventional 2D electron systems in semiconductor heterostructures. We have performed a systematic theoretical study of giant magnetoresistance oscillations induced in such structures by the microwave radiation [B2.14:3, B2.14:4, B2.14:5, B2.14:6, B1.8:4, B1.8:6, B1.8:12]. In ultra-high-mobility structures these oscillations lead to formation of regions of zero-resistance states.   Using the quantum kinetic equation framework, we have classified the mechanisms of the influence of the radiation on the transport properties of 2D electrons in a transverse magnetic field and evaluated the microwave-induced magnetoresistance. Our results are in agreement with key observations by a number of leading experimental groups worldwide. The methods we have developed in course of this study will be used in our research on optoelelctronic and non-equilibrium properties of graphene nanostructures.

In Ref. [B1.8:13] quantum magnetooscillations in the microwave absorption and dynamic Shubnikov-de Haas oscillations were studied experimentally in a high mobility 2DEG. For this purpose a sensitive high-Q cavity technique was used and a special setup to avoid undesirable magnetoplasmon effects masking the quantum oscillations was developed. Our theory describes experimental results for the microwave-induced resistance oscillations (MIRO) and for the quantum magneto-absorption (QMA) oscillations on the same wafer with the same value of the quantum relaxation time and without any further fitting parameters (Fig.19). This provides a strong experimental support to our theory of MIRO and QMA based on inter-Landau-level transitions. This success paves the way for the development of the theory for graphene (work in progress) that will take into account the peculiar (non-equidistant) spectrum of Landau levels in this material (Fig.19, right).
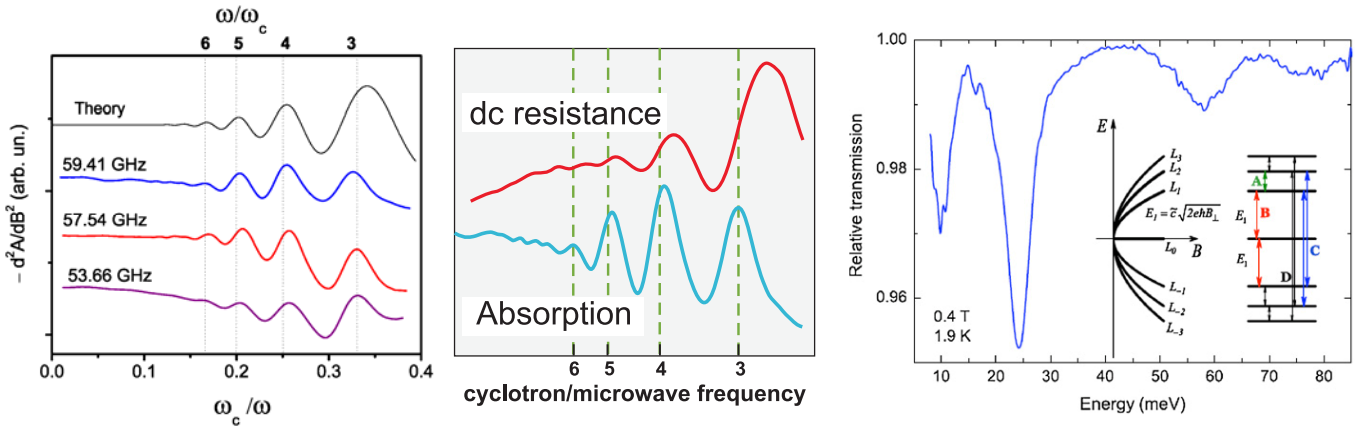
Fig. 19. *Left and middle:* Disorder-assisted microwave absorption between distant Landau levels leads to quantum magnetooscillations in absorption, as confirmed experimentally [B1.8:13]. The related mechanism is in the origin of microwave-induced resistance oscillations and zero-resistance states. *Right:* Non-equidistant spectrum of Landau levels in graphene [17] is important for magnetooptic and non-equilibrium properties of graphene.

The work [B1.8:5] was motivated by a recent experiment on quantum Hall structures with strongly asymmetric contact configuration that discovered microwave-induced photocurrent and photovoltage magnetooscillations in the absence of dc driving. We showed that in an irradiated sample the Landau quantization leads to violation of the Einstein relation between the dcconductivity and diffusion coefficient. Then, in the presence of a built-in electric field in a sample, the microwave illumination causes photo-galvanic signals which oscillate as a function of

magnetic field with the period determined by the ratio of the microwave frequency to the cyclotron frequency (Fig.20), as observed in the experiment. The experimental observation of the effect requires an asymmetry in contact geometry or in material composition of two contacts which determines the direction of the current. At the same time, the obtained current voltage characteristics are shown to be independent of detailed potential profile in the sample provided the relative change in the electron density across the sample remains small.
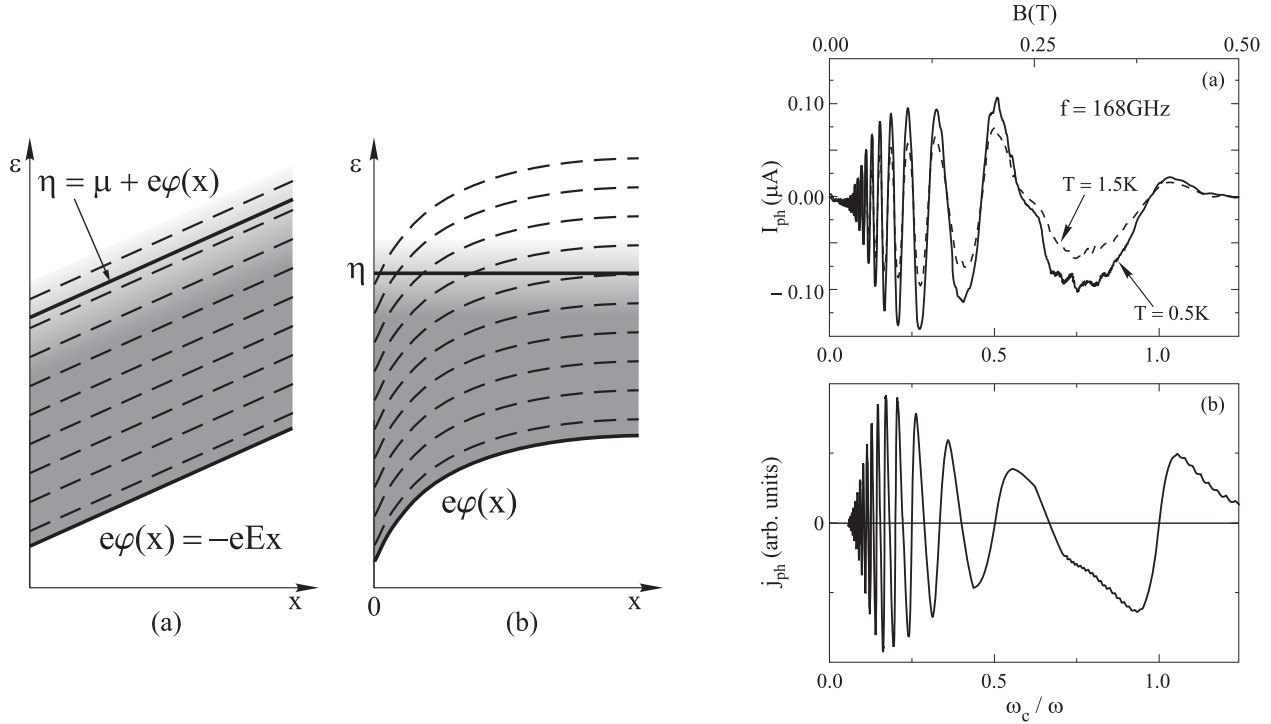
Fig. 20. *Left:* Distribution function of 2D electrons and Landau levels in (a) a non-equilibrium state with a constant electric field E in an infinite 2DEG and (b) an equilibrium finite 2DEG with a built-in electric field near a contact. *Right:* Microwave-induced photocurrent between the Corbino-like internal and strip-like external contact vs. magnetic field: (a) experiment [17], (b) theory [B1.8:5].

Cooperations

The work in B1.8 is carried out in cooperation with several CFN projects:
- Experimental studies are performed in KIT shared research group "Electronic properties of graphene" (Danneau) and in B2.7, C4.1 (von Löhneysen)
- Within B1.7 (Schön) numerical simulations of graphene are carried out.
- Transport and optics of nanotube-based carbon nanostructures are studied in B1.9 (Krupke) and in C3.2 (Kappes).
- Within C4.11 (Wölfle/Evers) and C3.11 (Evers) ab initio modeling of nanomechanical and electronic properties of graphene is performed.

We also maintain close contacts and cooperation with leading theoretical (Lancaster, Madrid, Würzburg, Edinburgh, Tel Aviv) and experimental (Manchester, Stuttgart, Exeter, Delft, Geneva, Grenoble, Minneapolis, Chernogolovka) groups.

References

- own work with complete titles -

[1]   A.K.Geim and K.S. Novoselov, Nature Materials **6**, 183-191 (2007).

[2]   K.S. Novoselov, A.K. Geim, S.V. Morozov, D. Jiang, Y. Zhang, S.V. Dubonos, I.V. Grigorieva, and A.A. Firsov, Science **306**, 666 (2004).

[3]   K.S. Novoselov, D. Jiang, T. Booth, V.V. Khotkevich, S.M. Morozov, and A.K. Geim, PNAS **102**, 10451 (2005).

[4]   K.S. Novoselov, A.K. Geim, S.V. Morozov, D. Jiang, M.I. Katsnelson, I.V. Grigorieva, S.V. Dubonos and A.A. Firsov, Nature **438**, 197 (2005).

[5]   Y. Zhang, Y.-W. Tan, H. L. Stormer and P. Kim, Nature **438**, 201 (2005); Y.-W. Tan, Y. Zhang,   H.L. Stormer, and P. Kim, Eur. Phys. J. Special Topics, **148**, 15 (2007).

[6]   P.M. Ostrovsky, I.V. Gornyi, and A.D. Mirlin, *Electron transport in disordered graphene*, Phys. Rev. B **74**, 235443 (2006).

[7]   A.H. Castro Neto, F. Guinea, N.M.R. Peres, K.S. Novoselov, and A.K. Geim, Rev. Mod. Phys. **81**, 109 (2009)

[8]   J.H. Bardarson, J. Tworzydlo, P.W. Brouwer, and C.W.J. Beenakker, Phys. Rev. Lett. **99**, 106801 (2007); K. Nomura, M. Koshino, and S. Ryu, Phys. Rev. Lett. **99**, 146806 (2007).

[9]   F. Evers and A.D. Mirlin, *Anderson transitions*, Rev. Mod. Phys. **80**, 1355 (2008).

[10]   J. Tworzydlo, B. Trauzettel, M. Titov, A. Rycerz, and C.W.J. Beenakker, Phys. Rev. Lett. **96**,   246802 (2006).

[11]   R. Danneau, F. Wu, M.F. Craciun, S. Russo, M.Y. Tomi, J. Salmilehto, A.F. Morpurgo, and P.J. Hakonen, Phys. Rev. Lett. **100**, 196802 (2008); Journ. Low Temp. Phys. **153**, 374 (2008).

[12]   P. San-Jose, E. Prada, and D.S. Golubev, Phys. Rev. B **76**, 195445 (2007).

[13]   J. Tworzydlo, C.W. Groth, and C.W. J. Beenakker, Phys. Rev. B **78**, 235438 (2008)

[14]   J. Schelter, P. M. Ostrovsky, I. V. Gornyi, B. Trauzettel, and M. Titov, *"Color-dependent conductance of graphene with adatoms"*, preprint arXiv:1011.4048, submitted to Physical Review Letters.

[15] J. Bardarson, M. Titov, and P.W. Brouwer, Phys. Rev. Lett. **102**, 226803 (2009).

[16] M. Schuett, P.M. Ostrovsky, I.V. Gornyi, and A.D. Mirlin, *"Coulomb interaction in graphene: Relaxation rates and transport"*, preprint arXiv:1011.5217, submitted to Physical Review B.

[17] M. Orlita and M. Potemski, Semicond. Sci. Technol. **25**, 063001 (2010).

[18] S.I. Dorozhkin et al., Phys. Rev. Lett. **102**, 036602 (2009).